Journal of Sound and Vibration 328 (2009) 411–427

Contents lists available at ScienceDirect

Journal of Sound and Vibration

journal homepage: www.elsevier.com/locate/jsvi

Structural damage detection using enhanced damage locating vector method with limited wireless sensors

S.T. Quek *, V.A. Tran, X.Y. Hou, W.H. Duan

Department of Civil Engineering, National University of Singapore, 1 Engineering Drive 2 #E1A-07-03, Singapore 117576, Singapore

ARTICLE INFO

Article history:
Received 3 February 2009
Received in revised form
10 August 2009
Accepted 18 August 2009
Handling Editor: L.G. Tham
Available online 9 September 2009

ABSTRACT

For detection of damage in structures, the damage locating vector (*DLV*) method is adapted to account for the different types and variations of internal forces and capacities along the length of each element by using the normalized cumulative energy instead of the normalized cumulative stress. To filter out the actual damaged elements from the identified set of potential damaged elements, an intersection scheme is proposed. A 2-D warehouse structure comprising beam and column elements with constant and varied cross-sectional areas, and truss elements is used to verify the enhancements to the *DLV* method. With wireless sensors being integrated into damage detection systems, practical issues need to be addressed in conjunction with the detection algorithm employed. For cases where raw signals are transmitted, the intermittent loss of data packets during transmission from the sensor nodes to the base station needs to be addressed. An algorithm to patch the lost data is proposed and when integrated with the *DLV* damage detection methodology, is experimentally shown to be feasible using a 3-D modular truss structure.

1. Introduction

As the number of structures increases, and as these structures age, issues of health, performance, maintenance and retrofitting become more prominent and pressing. Early detection of anomalies in structures through periodic or continuous monitoring is critical against catastrophe or sudden failure. Since damage alters the behavior of a structure under external loading, the change in behavior can be used to assess its "health" [1–4]. Non-destructive evaluation methods are preferred and have attracted many investigations [5,6]. Existing non-destructive damage detection algorithms are either over a global [7,8] or local domain [9–11] while the structural response used to assess its damage is either static [12,13] or dynamic [14–17].

Amongst the global level methods, the damage locating vector (*DLV*) method [7] has high practical potential. It is flexibility-based and involves the determination of a set of static load vectors, denoted as *DLV*, such that it creates zero stresses in the damaged elements when applied onto the reference structure. The *DLV* vector is extracted from the difference in structural flexibility matrices (formulated with respect to the sensor locations) between the reference and the damaged states [7,18]. The feasibility of the method has been illustrated numerically [7] and experimentally [19] using truss structures. To extend the applicability of the method, two enhancements are incorporated in this paper. Firstly, a composite measure is introduced within the *DLV* framework; for example, in a frame structure, the moment, shear, axial force, and their variations along each element length relative to element capacity should be jointly considered when

* Corresponding author.
E-mail address: cveqst@nus.edu.sg (S.T. Quek).

0022-460X/$ - see front matter © 2009 Elsevier Ltd. All rights reserved.
doi:10.1016/j.jsv.2009.08.018

assessing damage. Secondly, the *DLV* method identifies a set of potential damaged elements which usually contains both the actual damaged and some undamaged elements. If the number of sensors available for use is limited, the set may contain a sizable number of undamaged elements. An algorithm is proposed herein to sieve out the damaged elements.

Recently, wireless sensor technology has contributed to new developments in structural damage detection as there are significant advantages over wired sensors [20]. Issues related to adaptation and practical implementation of wireless sensor systems, such as power supply, network management, cross-talk, data integrity and transmission speed are being studied. The research and implementation of the *DLV* methodology have to take into account the possible use of wireless sensors and their associated practical issues. Though the data captured on board by the wireless sensors has been digitized, transmitting data packets from various sensor nodes to the base station using radio frequency (RF) commonly experiences intermittent loss. The causes of data loss may be explained by (a) data packets from more than one sensor reach the base station simultaneously; (b) distances between the sensor nodes and the base station are out of the communication range; and (c) acknowledgement (ACK) messages of the lost packets are over-written. If the ACK messages indicating the lost packet numbers are not received by the sensor node, the lost packets are not resent. The data loss phenomenon has been experimentally examined by Nagayama [21] which reported that the loss percentage is random and can be as high as 86 percent. The loss percentage of 20 percent found in the experiment can pose a huge challenge in the application of WSN for reliable structural damage detection [21]. Ongoing research has been carrying out to improve the hardware, software and transmission topology to mitigate the loss of data [22–24]. One way is to have on-board storage to accumulate the data and then Fourier transformed through a firmware before transmitting the amplitude, frequency and phase information to the base station. However, this is not available commercially and minor problems still exist; hence, this innovation is not considered in this paper. Instead, the numerical reconstruction of lost data in relation to structural damage identification using the *DLV* method will be explored.

In summary, the three main features of this paper are: (a) the use of the normalized cumulative energy (*NCE*) for each element as the parameter to identify damaged elements via the *DLV* method; (b) an intersection scheme to extract the set of actual damaged elements from the set of potential damaged elements (*PDE*), especially when limited number of sensors are used; and (c) an algorithm for data re-construction when wireless sensors are used in conjunction with the *DLV* method for structural damage detection. The feasibility of these enhancements is verified numerically using simulated data from a 2-D warehouse frame example and experimentally using physically measured data from a 3-D modular truss structure.

2. Enhancement to the *DLV* method

2.1. Normalized cumulative energy

Consider a linear elastic structure with *ns* sensors attached. Let $\mathbf{F}_u$ and $\mathbf{F}_d$ denote the $(ns \times ns)$ flexibility matrices constructed with respect to the *ns* sensor locations for the reference and the damaged structures, respectively. A $(ns \times 1)$ static load vector $\mathbf{P}$ $(\neq \mathbf{0})$, which satisfies the work done equation

$$0.5\mathbf{P}^{\mathrm{T}}(\mathbf{F}_d\mathbf{P}) = 0.5\mathbf{P}^{\mathrm{T}}(\mathbf{F}_u\mathbf{P}) \quad \text{or} \quad (\mathbf{F}_d - \mathbf{F}_u)\mathbf{P} = \mathbf{F}_\Delta\mathbf{P} = 0 \tag{1}$$

can be derived by performing a singular value decomposition (*SVD*) on $\mathbf{F}_\Delta$

$$\mathbf{F}_\Delta \xrightarrow{SVD} \mathbf{U}\cdot\mathbf{\Sigma}\cdot\mathbf{V}^{\mathrm{T}} = [\mathbf{U}_1 \ \ \mathbf{U}_0]\begin{bmatrix}\mathbf{\Sigma}_1 & \mathbf{0}\\ \mathbf{0} & \mathbf{0}\end{bmatrix}[\mathbf{V}_1 \ \ \mathbf{V}_0]^{\mathrm{T}} \tag{2}$$

This hinges on the orthonormal property of $\mathbf{V}$, where post-multiplying Eq. (2) by $\mathbf{V}$ on both sides gives

$$[\mathbf{F}_\Delta\mathbf{V}_1 \ \ \mathbf{F}_\Delta\mathbf{V}_0] = [\mathbf{U}_1\mathbf{\Sigma}_1 \ \ \mathbf{0}] \tag{3}$$

from which $\mathbf{F}_\Delta\mathbf{V}_0=\mathbf{0}$. Each column of $\mathbf{V}_0$ is a feasible solution to Eq. (1), and is by definition a *DLV* since the work done by this force vector on the structural changes is zero. The columns of $\mathbf{V}_0$ constitute a set of *DLV*s, where the number of columns in $\mathbf{V}_0$, denoted as *ndlv*, is less than *ns*. If column *i* of $\mathbf{V}_0$ is applied onto the reference structure, then the energy induced in element *j* of the structure is given by

$$\Xi_{ji} = \int_{L_j}\frac{M_{ji}^2}{2E_jI_j}\,\mathrm{d}s + \int_{L_j}\nu\frac{Q_{ji}^2}{2G_jA_j}\,\mathrm{d}s + \int_{L_j}\frac{N_{ji}^2}{2E_jA_j}\,\mathrm{d}s \tag{4}$$

where for element *j*, M_{ji}, Q_{ji}, N_{ji} are its internal moment, shear and axial force, respectively, due to column *i* of the *DLV*; L_j its length; ν its Poisson's ratio and E_jI_j, G_jA_j, E_jA_j its flexural, shear, and axial stiffness, respectively, in which E_j is its Young's modulus and G_j its shear modulus.

The *NCE* of element *j* is computed as

$$\overline{\Xi}_j = \frac{\Xi_j}{\Xi_{\max}} \tag{5}$$

where $\Xi_j = \sum_{i=1}^{ndlv}\Xi_{ji}$ and $\Xi_{\max} = \max_{all\ j}(\Xi_j)$. Physically, the *NCE* of element *j* is the normalized sum of internal work done on element *j* by the system of forces defined by the *DLV*s. Although the maximum sum of internal work is chosen as the

normalizing base (resulting in a maximum value of 1 for the element in the structure with the highest sum), an alternative normalization base is the sum of the total internal work done by all elements. If the latter is used, then the *NCE* of element *j* is physically the fraction contribution by this element to the total work done on the structure.

For truss structure, Eq. (4) becomes

$$\Xi_{ji} = \int_{L_j} \frac{N_{ji}^2}{2E_jA_j}\,\mathrm{d}s = \frac{N_{ji}^2 L_j}{2E_jA_j} = \sigma_{ji}^2 \frac{A_jL_j}{2E_j} \tag{6}$$

where σ_{ji} is the stress induced in element *j* by column *i* of $\mathbf{V}_0$. Based on Eq. (6),

$$\sigma_{ji} = \sqrt{\Xi_{ji} \times \frac{2E_j}{A_jL_j}} \tag{7}$$

From Eqs. (5) and (7), it can be deduced that the *NCS* in the original *DLV* method proposed by Bernal [7] and the *NCE* are not exactly the same. If the entire truss structure is composed of elements with the same moduli, lengths and cross-sectional areas, *NCE* is equal to the square of *NCS*.

The set of *PDE* comprises those elements with $\overline{\Xi}_j = 0$. In practice, due to the presence of noise and uncertainties, the *NCE* of damaged elements may not exactly be zero and a non-zero threshold is needed for practical applications. Based on the study by Sim et al. [25], if the value of 0.1 is used as the *NCS* threshold, then the probability of "false negative" (corresponding to the case when the damaged element is not within the set of identified *PDE*) is less than 5 percent assuming that the Young's moduli of all elements are statistically independent variables, each with a coefficient of variation, δ_E, of 10 percent. The same basis is adopted in this paper and the square value of the *NCS* threshold value is employed as *NCE* threshold. Based on the limited numerical and experimental examples performed by the authors, the value of 0.01 has been proven to be robust so far.

The *SVD* performed using Eq. (2) is based on the flexibility matrix and the resulting *DLV*s have force as the physical quantity. If the stiffness matrix is used instead, then the resulting *DLV*s obtained after performing *SVD* have displacement as the physical quantity. Applying these *DLV*s onto the reference structure as nodal displacement vectors, the structural internal forces can be computed. The *NCE* of each element is calculated following Eqs. (4) and (5) and used as the parameter to assess damage.

2.2. Intersection scheme to identify actual damaged elements

In the *DLV* method, if limited number of sensors is used, the set of *PDE* identified would contain some undamaged elements [7]. A scheme is formulated in this section to filter out the actual damaged elements by taking the intersection of all potential sets derived using data from various combinations of sensors. The scheme is summarized in Fig. 1.

Starting with *ns* sensors, a set of *PDE* is first computed and denoted as the current intersected damage set (*IDS*). Next, by using only data from *ns*-1 sensors, another set of *PDE* can be identified. By taking the common elements from this *PDE* and the current *IDS*, a new *IDS* is obtained. This procedure can be repeated for a different set of *ns*-1 sensors (since there are *ns* possible sets of *ns*-1 sensors) to get a new *IDS*. If the current and the new *IDS* are identical, the elements in the new *IDS* are identified as the actual damaged elements and the identification process is considered as completed. The process is also terminated if the new *IDS* is a null set, implying that there is no damaged element in the structure. If 2 consecutive *IDS* are not identical and the combinations of *ns*-1 sensors are exhausted, then combinations of *ns*-2 sensors are next considered until the criterion of 2 consecutive repeated *IDS* is met. The termination criterion can be increased to require a higher number of consecutive identical *IDS* to ensure robustness of the method at the expense of computational cost. Based on extensive study with different numerical examples, including data with added noise, it is found that the 2 identical consecutive *IDS* criterion is robust.

The scheme works provided that *ns* is greater than 2 since at least 2 measurements are required to form a matrix before any *SVD* can be performed to compute the *DLV*. With *ns*=2, only 1 set of *PDE* can be computed and no subsequent combination of sensors is available to filter out the actual damaged elements.

2.3. Formulating structural stiffness matrix

To obtain the *DLV*, either structural flexibility or stiffness matrix with *DOF* at sensor locations must be available. In the original *DLV* method, the flexibility matrix at sensor locations is formulated based on the eigensystem realization algorithm (*ERA*) method [26–28] in conjunction with an algorithm to compute flexibility coefficients from state space results [18] assuming that there is at least 1 collocated sensor-actuator pair. This requirement can be relaxed for the case where adding a known mass to the structure is possible or the "mass" matrix does not change when the structure changes from the reference to the damaged state [29,30]. In this section, a direct method is proposed to formulate the structural stiffness matrix based solely on the measured accelerations at the sensor locations, assuming that the mass matrix is known.

Consider an *n-DOF* structure with *ns* sensors attached. Assuming that *r* unknown input forces are acting on the structure, *nc* ($\geq$0) of which are collocated with the sensors. The locations of sensors and input forces are assumed known.

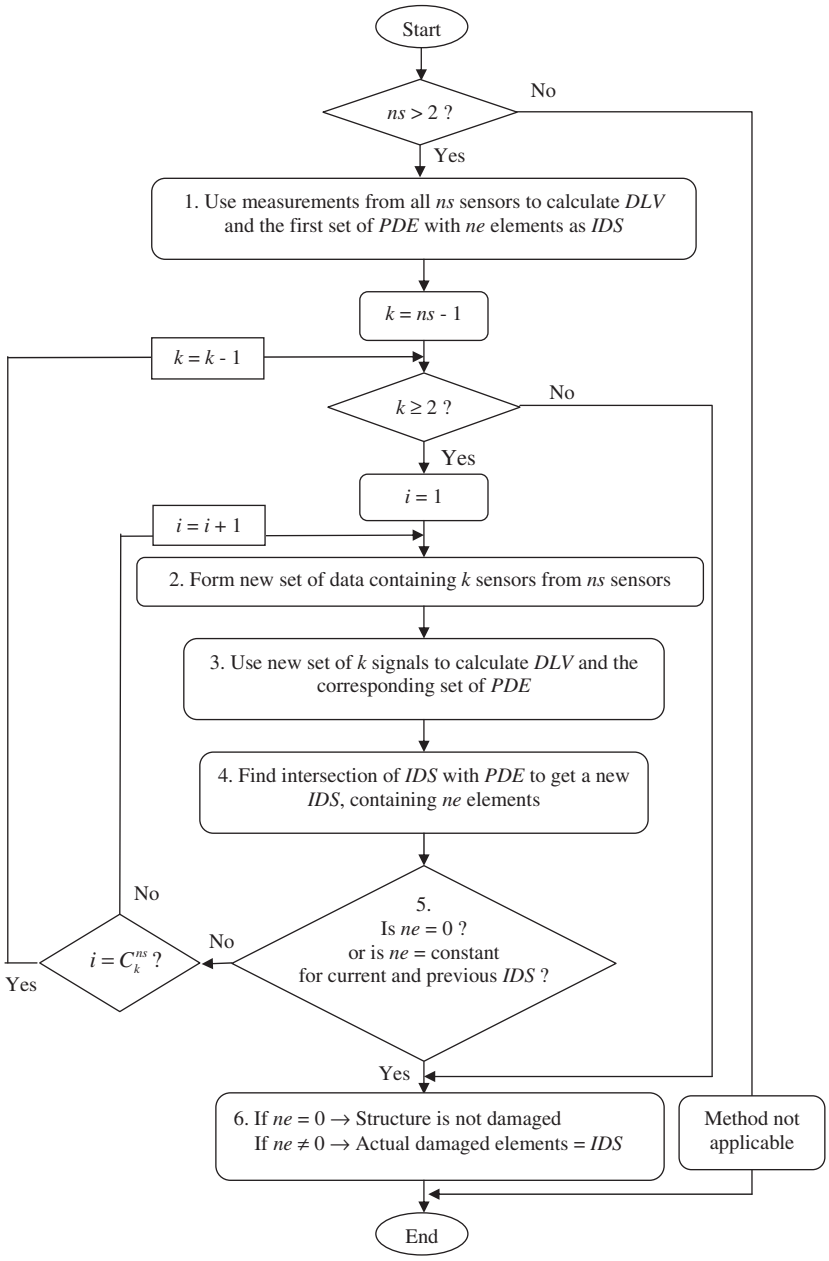

Fig. 1. Flow chart for intersection scheme to identify actual damaged elements.

The equation of motion of the structure can be expressed as

$$\mathbf{M}\ddot{\mathbf{d}} + \mathbf{D}_d\dot{\mathbf{d}} + \mathbf{K}\mathbf{d} = \mathbf{P} \tag{8}$$

where $\mathbf{M}$, $\mathbf{D}_d$, and $\mathbf{K}$ are the $(n \times n)$ mass, damping and stiffness matrices, respectively; $\ddot{\mathbf{d}}$, $\dot{\mathbf{d}}$ and $\mathbf{d}$ the $(n \times 1)$ acceleration, velocity and displacement vectors, respectively; and $\mathbf{P}=\mathbf{B}_2\mathbf{u}$ the $(n \times 1)$ applied force vector in which $\mathbf{B}_2$ is the input influence matrix to map the $(r \times 1)$ input force vector $\mathbf{u}$ to the structural *DOF*.

If a sampling time interval of Δt is used, then the structural displacement and velocity responses at time step j can be estimated using their values at step $(j-1)$ through the Newmark-β method as

$$\begin{cases} \dot{\mathbf{d}}_j = \dot{\mathbf{d}}_{j-1} + (1-\gamma)\cdot\Delta t\cdot\ddot{\mathbf{d}}_{j-1} + \gamma\cdot\Delta t\cdot\ddot{\mathbf{d}}_j \\ \mathbf{d}_j = \mathbf{d}_{j-1} + \Delta t\cdot\dot{\mathbf{d}}_{j-1} + (0.5-\beta)\cdot\Delta t^2\cdot\ddot{\mathbf{d}}_{j-1} + \beta\cdot\Delta t^2\cdot\ddot{\mathbf{d}}_j \end{cases} \tag{9}$$

where γ and β are the integration constants, taken as $\gamma = 0.50$, $\beta = 0.25$ which correspond to the case of constant average acceleration within Δt. Written in terms of the initial conditions $\mathbf{d}_1$ and $\dot{\mathbf{d}}_1$, and the accelerations (*ns* of which are measured and *n*−*ns* of which are not measured and to be solved up to time step *j*), Eq. (9) becomes

$$\begin{cases} \dot{\mathbf{d}}_j = \dot{\mathbf{d}}_1 + B_1 \sum_{i=1}^{j-1} (\ddot{\mathbf{d}}_i + \ddot{\mathbf{d}}_{i+1}) \\ \mathbf{d}_j = \mathbf{d}_1 + (j-1)\dot{\mathbf{d}}_1 \Delta t + C_1 \sum_{i=1}^{j-1} (\ddot{\mathbf{d}}_i + \ddot{\mathbf{d}}_{i+1}) + B_1 \Delta t \sum_{i=1}^{j-1} [(j-i-1)(\ddot{\mathbf{d}}_i + \ddot{\mathbf{d}}_{i+1})] \end{cases} \tag{10}$$

where $B_1 = 0.5\Delta t$, $C_1 = 0.25\Delta t^2$.

In theory, with k_1 time steps of measured accelerations, $k_1 n$ equations can be formulated using Eq. (8) as

$$\begin{cases} \mathbf{M}\ddot{\mathbf{d}}_1 + \mathbf{D}_d\dot{\mathbf{d}}_1 + \mathbf{K}\mathbf{d}_1 = \mathbf{P}_1 \\ \mathbf{M}\ddot{\mathbf{d}}_2 + \mathbf{D}_d\dot{\mathbf{d}}_2 + \mathbf{K}\mathbf{d}_2 = \mathbf{P}_2 \\ \cdots\cdots\cdots\cdots\cdots\cdots \\ \mathbf{M}\ddot{\mathbf{d}}_{k_1} + \mathbf{D}_d\dot{\mathbf{d}}_{k_1} + \mathbf{K}\mathbf{d}_{k_1} = \mathbf{P}_{k_1} \end{cases} \tag{11}$$

where subscripts $1, 2, \ldots, k_1$ denote time steps. Substituting Eq. (10) into (11), the unknowns in Eq. (11) include: (i) $2n$ initial conditions ($\mathbf{d}_1$ and $\dot{\mathbf{d}}_1$ for each of the *n-DOF*); (ii) $k_1(n-ns)$ accelerations which are not measured; (iii) $n(n+1)/2$ entries in each of $\mathbf{D}_d$ and $\mathbf{K}$, both of which are symmetric matrices; and (iv) $k_1 r$ unknown input forces. To solve for these unknowns and hence obtain $\mathbf{K}$, the number of time steps of acceleration data required is

$$k_1 n \geq n(n+1) + k_1(n-ns) + 2n + k_1 r \Rightarrow k_1 \geq \frac{n(n+3)}{ns-r} \tag{12}$$

It is observed from Eq. (12) that the number of time steps (k_1) depends on the number of *DOF* of structure (n), the number of excitation forces (r), and the number of sensors used (ns). Since Eq. (12) does not depend on the number of collocated sensor-actuator pairs (nc), the method overcomes the requirement that at least 1 collocated sensor-actuator pair must exist in the original *DLV* method.

Eq. (11) is a system of nonlinear equations which can be solved by either the Secant method [31] or the Newton–Raphson method [32]. The unknowns are explicitly given in Eq. (11) and hence the Jacobian matrix can be computed. The Newton–Raphson method is therefore employed using the parameters of the structure at the reference state as initial guess for the unknowns in $\mathbf{D}_d$ and $\mathbf{K}$ to obtain the solution numerically.

For a feel of the number of time steps required, a structure with 10 *DOF* (n=10), excited by 2 actuators (r=2) and monitored by 3 sensors (ns=3) gives $k_1 \geq 130$ whereas a structure with 50 *DOF* (n=50), excited by 2 actuators (r=2) and monitored by 8 sensors (ns=8) necessitates $k_1 \geq 442$.

The above derivation assumes that (i) $ns > r$ (or the number of unknown force time histories) and (ii) stiffness and damping do not change within these k_1 time steps. If $ns \leq r$ or the locations of the applied loads are not known, this method cannot be used. The smallest value for k_1 is (n+3). For cases where ns is small and r is not much smaller than ns, k_1 may be extremely large to make the method impractical. If stiffness and damping change slowly (less than 0.1 percent within k_1 time steps), then the values computed are averaged values otherwise the results may not represent the stiffness and damping matrices of the damaged structure. If the measured time histories are long, then consecutive segments of k_1 time steps of data may be used and the changes of $\mathbf{D}_d$ and $\mathbf{K}$ with time segments can be monitored. In fact, how the damage evolves with time may be captured, or if only the final state is of interest, the final $\mathbf{K}$ values can be used with the knowledge of whether it has stabilized. It is possible to track how damping and stiffness matrices vary with time with better resolution by using moving time segments at the expense of significantly larger computational effort.

The computation may be speeded up by considering equilibrium equations at *DOF* where there are no external excitations. Using this approach, only portions of damping and stiffness matrices are estimated. The remaining portions of damping and stiffness matrices and input forces are then computed using the above equations as a follow-on step. The savings in computational time is not worth the added complexity in the procedure and hence is not presented here.

3. Reconstruction of lost data for wireless sensor

Wireless sensors may be integrated into the *DLV* damage detection methodology in line with the advancement in sensor technology. Practical issues such as the loss of data during transmission of data packets from the sensor nodes to the base station need to be addressed in conjunction with the detection algorithm employed. The algorithm to reconstruct lost data presented below is performed individually for the signals of each sensor collected at the base station.

The idea behind the reconstruction procedure adopted here is that the complete signal (without loss) can be Fourier transformed into various discrete frequencies. If the proportion of data that is lost is not significant, then reconstruction is possible by making use of the available signal (says m points from a total of ξ points, that is, ξ-m points are lost which are set to zeroes) to identify the significant frequencies (says *nfreq* number of significant frequencies, $nfreq < 0.5\xi$). These

frequencies together with Fourier coefficients A_k determined by least-square fit of the m measured values (requiring that $m > nfreq$ or $m > 0.5\xi$) are then used to reconstruct an approximated complete signal using the following equation:

$$x_n = \frac{1}{\xi}\sum_{k=1}^{nfreq}\left[A_k \exp\left(\mathrm{j}n\frac{2\pi(k-1)}{\xi}\right)\right] \tag{13}$$

where j denotes the imaginary unit. The reconstructed signal now comprises measured values and lost values that have been computed using Eq. (13). Performing Fourier transformed on the reconstructed signal, a new set of significant frequencies which may not be the same as the previously identified significant frequencies is calculated. The latest set of frequencies will then be used as before to obtain the Fourier coefficients based on least-square fit of the m measured data points. A new signal can then be reconstructed and compared with the previously reconstructed signal. The relative difference, *Rerr*, between 2 consecutive reconstructed lost portions of the signal is computed as

$$Rerr = \sqrt{\frac{\sum_{k=1}^{\xi-m}(g_k^i - g_k^{i-1})^2}{\sum_{k=1}^{\xi-m}(g_k^i)^2}} \times 100 \text{ percent} \tag{14}$$

where g_k^i, g_k^{i-1} are the estimated lost values at iterations i and $(i-1)$, respectively. This procedure is iterated until *Rerr* is less than 1 percent. The proposed data reconstruction algorithm is summarized in Fig. 2.

For determining whether a frequency is significant, a threshold of 1 percent for the ratio between its power spectral values (*PSV*) and the maximum *PSV* in a signal is adopted. To estimate the error due to neglecting the insignificant frequencies, a numerical study is performed on a signal with 1600 data points sampled at a rate of 1 kHz as shown in Fig. 3. In theory, performing Fourier transformed on the signal, 800 frequencies and their corresponding Fourier coefficients can be obtained. By using only the significant frequencies with their corresponding Fourier coefficients, a complete signal can

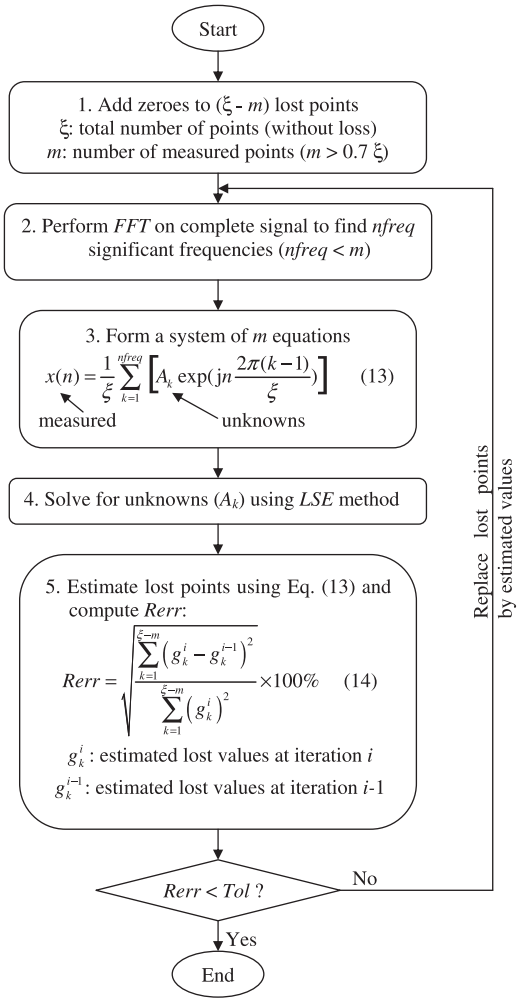

Fig. 2. Block diagram for lost data reconstruction algorithm.

be constructed using Eq. (13) and its relative error with respect to the actual signal estimated. If the threshold of 1 percent is employed to demarcate the significant frequencies, 762 frequencies (see Fig. 4a) are identified and used to reconstruct the signal, yielding a relative error of 0.9 percent (Fig. 4b). If a 5 percent relative error is considered acceptable, Fig. 4 indicates that a threshold of 20 percent to demarcate the significant frequencies is adequate. Note that this relative error is the difference between the reconstructed and the exact complete signals and is different from that of Eq. (14) which is the relative difference of lost portions between 2 consecutive reconstructed signals. Nevertheless, this gives a sense of the minimum *Rerr* that can be imposed in the reconstruction procedure.

To study the reliability of the reconstruction methodology, the same signal of 1600 data points in Fig. 3 is used where random portions of the data (multiples of 4 consecutive data points) are padded with zeroes to simulate the loss of data packets during RF transmission from the sensor nodes to the base station. The reconstruction procedure is then performed and the relative error plotted in Fig. 5. With threshold of 1 percent for both *Rerr* and the *PSV* to demarcate significant

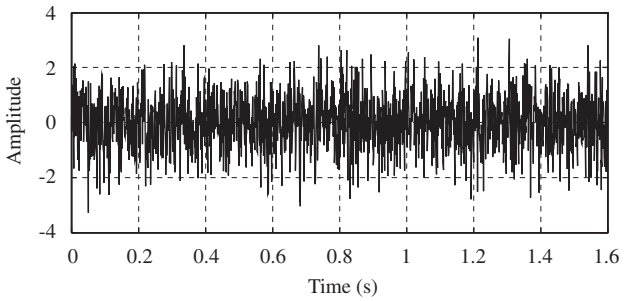

Fig. 3. Random signal with sampling rate of 1 kHz.

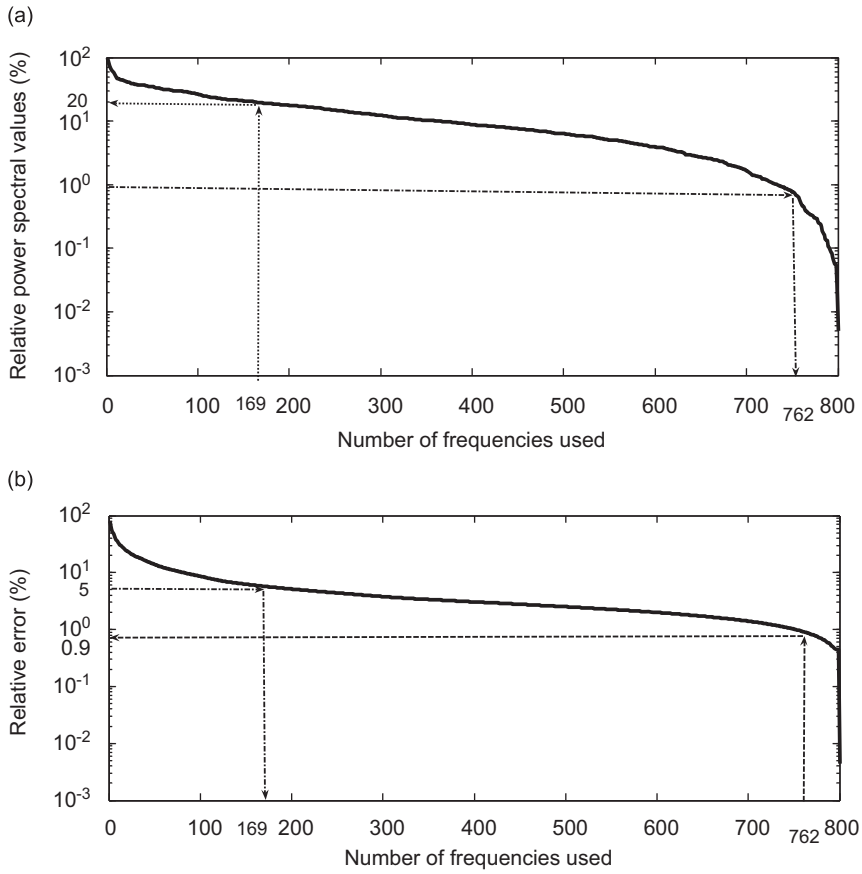

Fig. 4. Relationship between number of frequencies used and (a) relative power spectral value and (b) relative error between reconstructed and exact signals.

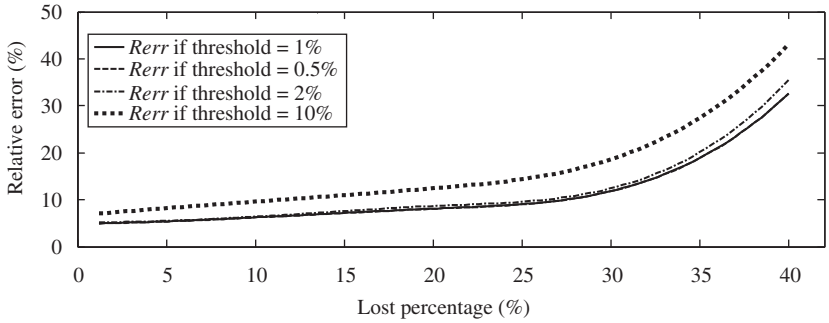

Fig. 5. Relationship between lost percentage and *Rerr* for different thresholds.

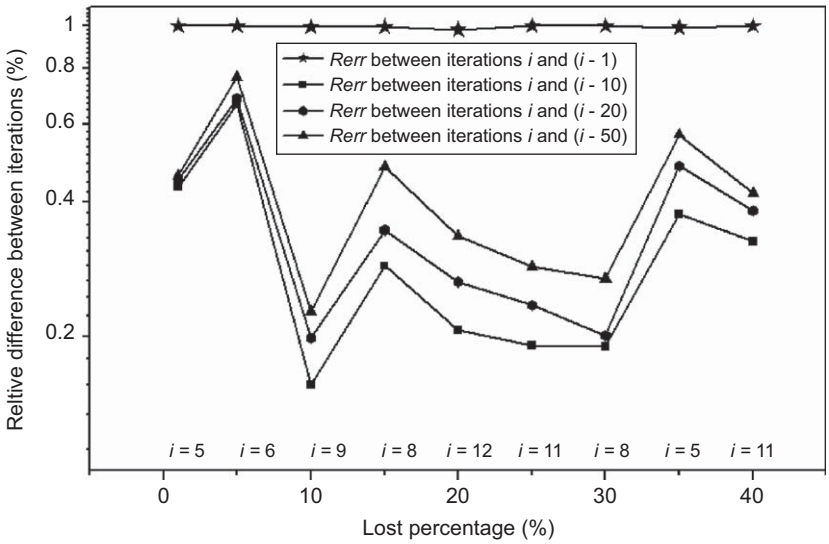

Fig. 6. Relative difference of lost portions with iterations.

frequencies, the minimum relative error for lost portions achievable is 5 percent. For data loss beyond 28 percent, the relative error using this reconstruction procedure grows exponentially from 10 percent, beyond which it becomes unattractive for practical applications. Hence, this reconstruction procedure is practical for approximately $m > 0.7\xi$, that is, less than 30 percent of the data is lost. The same signal is used to obtain results for thresholds of 10, 2 and 0.5 percent for both the significant frequencies and *Rerr*. The results in Fig. 5 show that the accuracy of the reconstructed signal is improved significantly when the threshold is reduced from 10 to 2 percent, but only slightly when it is reduced from 2 to 0.5 percent. Thus, the proposed value of 1 percent appears adequate. To investigate the robustness of the *Rerr* threshold of 1 percent to terminate the iteration in Eq. (14), the reconstruction process is iterated for 10, 20 and 50 additional cycles after the threshold of 1 percent is reached. Results in Fig. 6 testify that the relative differences between lost portions at iterations i and (i+10), (i+20), (i+50) show little improvement with the additional cycles of computation, indicating that 1 percent is a fairly optimal threshold.

If the raw signals where lost values are padded with zeroes for the lost data are employed to estimate the structural stiffness matrix and then used in the *DLV* method, no *DLV* is computed. It may be explained by the large error in the identified stiffness matrix induced by the poor quality of the measured signals. On the other hand, if the reconstructed signals are employed, the damaged element is detected correctly as will be illustrated through an example in Section 4.2.

4. Numerical and experimental verification

The use of *NCE* as damage indicator and the intersection scheme to identify actual damaged elements is illustrated numerically through a 2-D warehouse frame in Section 4.1. The algorithm for lost data reconstruction is verified using experimentally measured data via a 3-D modular truss structure in Section 4.2.

4.1. Numerical example of a warehouse frame structure

A 2-D warehouse frame shown in Fig. 7 is considered. The frame comprises (a) beams and columns with either constant or varied cross-sectional areas; and (b) truss members. The specifications for the frame members are listed in Table 1. Two cases of damage are investigated, namely element 14 is damaged, and elements (7, 14) are damaged. Damage is simulated by imposing a reduction of 20 percent in flexural stiffness (*EI*) of column element 7 whereas for truss member 14, a 20 percent reduction in axial stiffness (*EA*) is imposed. The structure is excited horizontally by a zero-mean white random load at node 9, and horizontal and vertical acceleration responses at nodes (4, 6, 8, 9, 10, 13) and (5, 7, 11, 12), respectively, are monitored.

For the case where element 14 is damaged, from 10 monitored acceleration responses, the method in Section 2.3 is used to formulate the structural stiffness matrix with respect to the sensor locations. Change in the stiffness matrix is then computed by comparing the identified and the reference stiffness matrices. Performing *SVD* on the change in the stiffness matrix, a set containing 9 *DLV*s is obtained. By applying these *DLV*s to the reference structural model as nodal displacement vectors, the *NCE* of all elements are computed and the set of *PDE* which includes elements (14, 17) is identified. Therefore, the current *IDS* contains elements (14, 17) and *ne*=2. By omitting data from readings of the sensor at node 4, the stiffness matrix at the remaining 9 sensor locations is computed based on the remaining 9 sensor readings following the method in Section 2.3. Comparing the identified and the reference stiffness matrices, the change in the stiffness matrix is computed. By performing *SVD* on the change in the stiffness matrix, another set containing 8 *DLV*s is identified. By applying these *DLV*s onto the reference structural model as nodal displacement vectors, the *NCE* of all elements are computed and the set of *PDE*

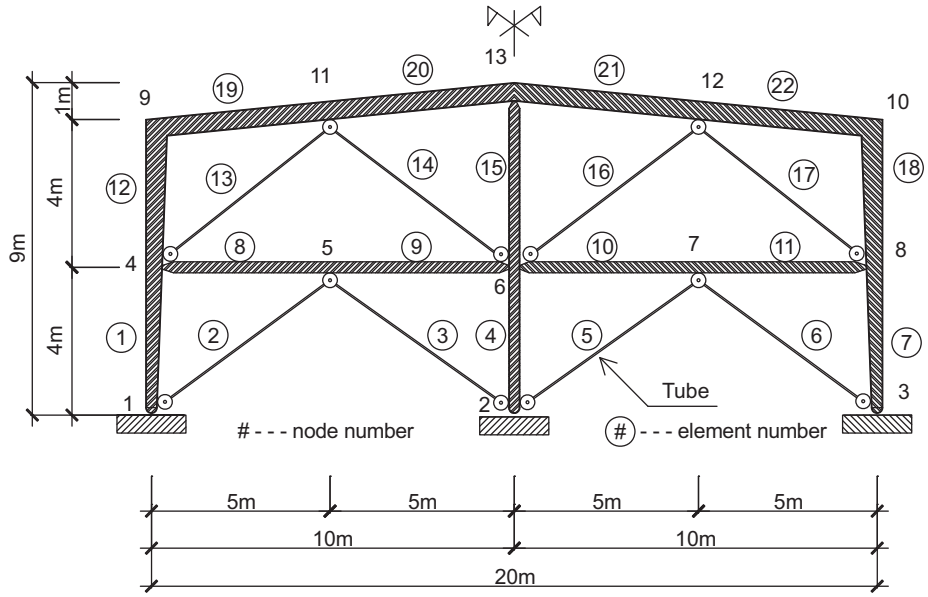

Fig. 7. Warehouse frame structure.

Table 1
Specifications for members of warehouse structure.

Element numbers		Height (mm)	Width (mm)	Flange thickness (mm)	Web thickness (mm)	Young's modulus (10^{11} Nm^{-2})	Moment of inertia (10^{-8} m^4)	Cross-sectional area (10^{-4} m^2)
1, 7	end 1	300	300	16	10	2.10	20,982	122.8
	end 2	450	300	16	10	2.10	51,312	137.8
12, 18	end 1	450	300	16	10	2.10	51,312	137.8
	end 2	600	300	16	10	2.10	97,145	152.8
4,15		300	300	16	10	2.10	20,982	122.8
19, 20, 21, 22		500	300	16	10	2.10	64,784	142.8
8, 9, 10, 11		300	300	16	10	2.10	20,982	122.8
2, 3, 5, 6, 13, 14, 16, 17		Tubular sections				2.10	4	2.0

Table 2
Damage detection of warehouse (element 14 damaged).

	Set of sensors includes sensors at nodes	No. of *DLV*	*PDE*	Eliminated elements	*IDS*	*ne*
ns=10	[4, 5, 6, 7, 8, 9, 10, 11, 12, 13]	9	[14, 17]		[14, 17]	2
k=*ns*−1=9						
i=1	[5, 6, 7, 8, 9, 10, 11, 12, 13]	8	[14]	17	[14]	1
i=2	[4, 5, 6, 7, 8, 9, 11, 12, 13]	8	[12, 14, 17]		[14]	1
i=3	[4, 6, 7, 8, 9, 10, 11, 12, 13]	8	[4, 14]		[14]	1
i=4	[4, 5, 7, 8, 9, 10, 11, 12, 13]	8	[1, 2, 7, 14, 20]		[14]	1
i=5	[4, 5, 6, 8, 9, 10, 11, 12, 13]	8	[12, 14]		[14]	1
i=6	[4, 5, 6, 7, 9, 10, 11, 12, 13]	8	[14, 16]		[14]	1
i=7	[4, 5, 6, 7, 8, 10, 11, 12, 13]	8	[14]		[14]	1
i=8	[4, 5, 6, 7, 8, 9, 10, 11, 12]	8	[12, 14, 16]		[14]	1
i=9	[4, 5, 6, 7, 8, 9, 10, 12, 13]	8	[12, 14]		[14]	1
i=10	[4, 5, 6, 7, 8, 9, 10, 11, 13]	8	[14, 17]		[14]	1

Table 3
Damage detection of warehouse (elements 7 and 14 damaged).

	Set of sensors includes sensors at nodes	No. of *DLV*	*PDE*	Eliminated elements	*IDS*	*ne*
ns=10	[4, 5, 6, 7, 8, 9, 10, 11, 12, 13]	9	[1, 4, 7, 13, 14]		[1, 4, 7, 13, 14]	5
k=*ns*−1=9						
i=1	[4, 5, 6, 7, 8, 9, 11, 12, 13]	8	[7, 12, 14]	1, 4, 13	[7,14]	2
i=2	[4, 5, 6, 7, 8, 10, 11, 12, 13]	8	[1, 7, 13, 14, 17]		[7,14]	2

which contains element 14 is identified. Intersecting the set of *PDE* and the current *IDS* which contains elements (14, 17) produces element 14 as the new *IDS* (*ne*=1). Similarly, by omitting the readings of the sensor at node 10 instead of the sensor at node 4, another set of *PDE* containing elements (12, 14, 16) is identified. Intersecting the identified *PDE* with the current *IDS* which contains element 14 only gives element 14 as the new *IDS* (*ne*=1). Since the *IDS* is the same for 2 consecutive steps, the iteration is terminated and the actual damaged element 14 is identified correctly. The procedure is summarized in the upper portion of Table 2. Similarly for the case where elements (7, 14) are damaged, the feasibility of the method is confirmed by the results in Table 3.

To demonstrate that 2 consecutive identical *IDS* is adequate to stop the iteration described in Section 2.2, the remaining 8 combinations resulting from omitting 1 sensor readings at a time are considered and the identified *PDE* are listed in the lower portion of Table 2 for the case where element 14 is damaged. The intersected damaged set *IDS* contains only element 14 for all cases, confirming the suitability of the proposed criterion. The same computation is performed for the case where elements (7, 14) are damaged and yields the same conclusion although the results are not presented here.

To investigate the effect of noise on the performance of the proposed methodology, the above example is used and zero-mean white noise with root mean square (*RMS*) of (i) 5 percent; and (ii) 10 percent of the *RMS* of the response signal is added to all simulated response accelerations to generate contaminated responses. For the case of 5 percent noise, from the contaminated responses of 10 sensors, the method in Section 2.3 is employed to calculate the structural stiffness matrix. By comparing the identified and the reference stiffness matrices, the change in the stiffness matrix is computed. Applying *SVD* on the change in stiffness matrix, a set containing 7 *DLV*s is computed. Applying these *DLV*s onto the reference structure as nodal displacement vectors, the *NCE* of all elements are calculated and the first set of *PDE* which includes 6 elements (4, 6, 12, 13, 14, 17) is identified. These 6 elements are assigned the current *IDS* (*ne*=6). By omitting readings of the sensor at node 4 and employing the method in Section 2.3 on the remaining 9 sensor readings, the stiffness matrix with respect to the remaining 9 sensor locations is computed. Comparing the identified and the reference stiffness matrices, the change in the stiffness matrix is evaluated, based on which *SVD* is performed to identify another set containing 5 *DLV*s. Applying these *DLV*s onto the reference structural model as nodal displacement vectors, the *NCE* of all elements are evaluated and the set of *PDE* which includes elements (1, 8, 10, 14) is identified. Taking the intersection between the set of *PDE* and the current *IDS* which contains elements (4, 6, 12, 13, 14, 17) gives element 14 as the new *IDS* (*ne*=1). Similarly, by omitting the readings of the sensor at node 10 instead of the sensor at node 4 another set of *PDE* comprising elements (6, 14, 16) is identified. The intersection of the set of *PDE* and the current *IDS* which contains element 14 only produces element 14 as the new *IDS* (*ne*=1). Since the *IDS* for the 2 consecutive steps are identical, the iteration is stopped with the conclusion that element 14 is

Table 4
Damage detection of warehouse with 5% noise added (element 14 damaged).

	Set of sensors includes sensors at nodes	No. of *DLV*	*PDE*	Eliminated elements	*IDS*	*ne*
ns=10	[4, 5, 6, 7, 8, 9, 10, 11, 12, 13]	7	[4, 6, 12, 13, 14, 17]		[4, 6, 12, 13, 14, 17]	6
k=*ns*−1=9						
i=1	[5, 6, 7, 8, 9, 10, 11, 12, 13]	5	[1, 8, 10, 14]	4, 6, 12, 13, 17	[14]	1
i=2	[4, 5, 6, 7, 8, 9, 11, 12, 13]	5	[5, 14, 16]		[14]	1
i=3	[4, 6, 7, 8, 9, 10, 11, 12, 13]	5	[14]		[14]	1
i=4	[4, 5, 7, 8, 9, 10, 11, 12, 13]	5	[7, 14]		[14]	1
i=5	[4, 5, 6, 8, 9, 10, 11, 12, 13]	5	[5, 6, 14]		[14]	1
i=6	[4, 5, 6, 7, 9, 10, 11, 12, 13]	5	[10, 11, 12, 14, 15]		[14]	1
i=7	[4, 5, 6, 7, 8, 10, 11, 12, 13]	5	[1, 8, 9, 14, 16, 21]		[14]	1
i=8	[4, 5, 6, 7, 8, 9, 10, 11, 12]	5	[14, 15, 19, 20]		[14]	1
i=9	[4, 5, 6, 7, 8, 9, 10, 12, 13]	5	[14, 18]		[14]	1
i=10	[4, 5, 6, 7, 8, 9, 10, 11, 13]	5	[7, 14]		[14]	1

Table 5
Damage detection of warehouse with 10% noise added (element 14 damaged).

	Set of sensors includes sensors at nodes	No. of *DLV*	*PDE*	Eliminated elements	*IDS*	*ne*
ns=10	[4, 5, 6, 7, 8, 9, 10, 11, 12, 13]	5	[3, 8, 9, 13, 14, 16, 18, 20, 21, 22]		[3, 8, 9, 13, 14, 16, 18, 20, 21, 22]	10
k=*ns*−1=9						
i=1	[5, 6, 7, 8, 9, 10, 11, 12, 13]	4	[1, 4, 7, 14, 17]	3, 8, 9, 13, 16, 18, 20, 21, 22	[14]	1
i=2	[4, 5, 6, 7, 8, 9, 11, 12, 13]	4	[5, 7, 14, 19]		[14]	1
i=3	[4, 6, 7, 8, 9, 10, 11, 12, 13]	4	[14, 15]		[14]	1
i=4	[4, 5, 7, 8, 9, 10, 11, 12, 13]	4	[4, 7, 11, 12, 14, 16, 20]		[14]	1
i=5	[4, 5, 6, 8, 9, 10, 11, 12, 13]	4	[6, 14]		[14]	1
i=6	[4, 5, 6, 7, 9, 10, 11, 12, 13]	4	[2, 4, 5, 6, 14, 17]		[14]	1
i=7	[4, 5, 6, 7, 8, 10, 11, 12, 13]	4	[1, 3, 5, 6, 14, 15, 17]		[14]	1
i=8	[4, 5, 6, 7, 8, 9, 10, 11, 12]	4	[4, 5, 7, 14, 15, 17, 19]		[14]	1
i=9	[4, 5, 6, 7, 8, 9, 10, 12, 13]	4	[10, 11, 14, 15, 18]		[14]	1
i=10	[4, 5, 6, 7, 8, 9, 10, 11, 13]	4	[1, 4, 7, 9, 12, 14, 17]		[14]	1

damaged which matches the actual case. The procedure is summarized in the upper portion of Table 4. Performing the same procedure for the other 8 combinatorial sets of sensors by dropping 1 sensor record each time, the results in the lower portion of Table 4 confirm that only element 14 is damaged, reinforcing the criterion of 2 consecutive identical *IDS* to stop the iteration in Section 2.2. The same computation is performed for the case of 10 percent noise and the results in Table 5 support the feasibility of the proposed methodologies. Similar trends are observed for the case where elements (7, 14) are damaged although the results are not presented here.

It is observed that the number of *DLV*s computed from the contaminated data is less than that computed from the pure data. If the noise level goes beyond a certain threshold, no *DLV* may be computed. The determination of the threshold noise level is not covered in this paper.

4.2. Experimental verification using truss structure

A 3-D modular truss structure comprising 23 aluminum tubes and 1 pre-tensioned cable is used in this experiment (see Fig. 8). The geometrical and material properties of the truss members are listed in Table 6 whereas element and node numbers are plotted in Fig. 9. Damage in the structure is simulated by cutting the pre-tensioned cable member mid-way through the test. Zero-mean white random load on the truss is generated using a shaker with capacity of 100 lbs (334 N) and the acceleration responses of the truss are captured by 6 wireless sensors (the senor locations are given in Fig. 8).

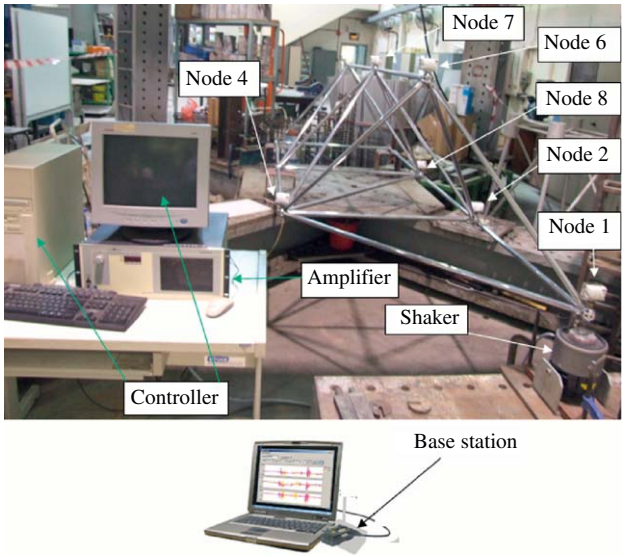

Fig. 8. Experimental set-up.

Table 6
Geometric and material properties of truss members.

	Aluminum tubular members	Pre-tensioned cable members
Outside diameter (mm)	20.0	4.0
Thickness (mm)	1.0	–
Young's modulus (N/m^2)	6.8×10^{10}	1.6×10^{11}
Mass density (kg/m^3)	2690.0	7500.0
Pre-tensioned force (N)	–	2000.0

Note: "–" means not applicable.

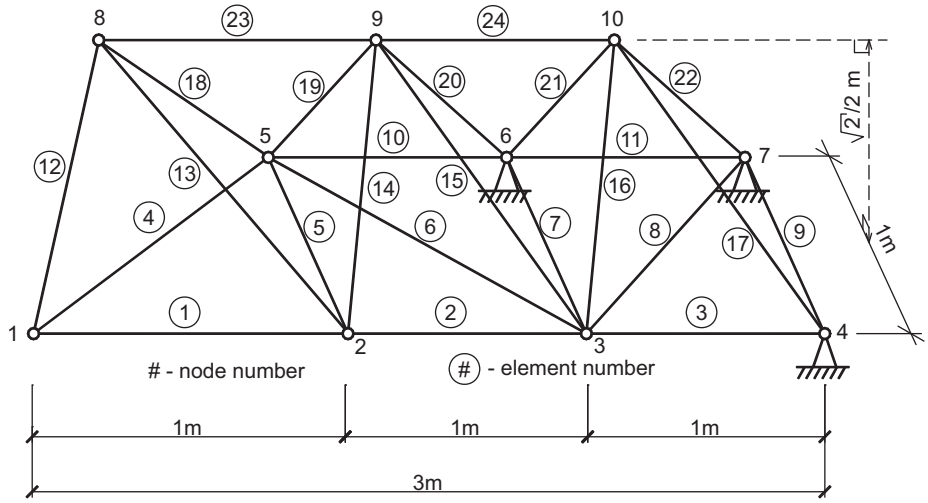

Fig. 9. Element and node numbers for experimental truss structure.

The lost percentages of the acceleration responses captured by the 6 wireless sensors are given in the upper portion of Table 7, indicating that the loss of data packets are in fact random and not synchronized which agree well with the findings by Nagayama [21]. With the lost percentage ranging from 19 to 24.5 percent, reconstruction error of the lost portions is expected to fall between 8 and 9 percent based on Fig. 5. The reconstruction procedure to estimate lost data values measured by each wireless sensors is applied and the information is summarized in the lower portion of Table 7. It can

Table 7
Computational details for signal reconstruction at 6 sensor nodes.

	Node 1	Node 2	Node 4	Node 6	Node 7	Node 8
Number of lost points	352	380	392	376	304	372
Total number of points	1600	1600	1600	1600	1600	1600
Lost percentage (%)	22.00	23.75	24.50	23.50	19.00	23.25
Number of iterations	12	14	14	11	14	10
Number of frequencies used in the last iteration	479	467	495	367	479	343
Relative error at the last iteration (%)	0.62	0.33	0.55	0.72	0.87	0.83

Note: See Fig. 8 for sensor node locations.

be observed from Table 7 that the number of iterations required is small, ranging from 10 to 14, and is not proportional to the lost percentages, as the distribution of the lost packets is another controlling parameter. The results for sensor node 4 are shown in Fig. 10. Fig. 10a gives the signal captured by wireless sensor at sensor node 4 including an insert to show an example of the lost data. Fig. 10b gives a better indication of the locations of the lost data points based on the "corrected" values. Fig. 10c compares in frequency domain the raw signal against the reconstructed signal which shows no drastic change in the trend or general characteristics.

From the reconstructed accelerations, 15 segments, each of which contains 109 time steps, can be used to estimate the structural stiffness coefficients and selected results are plotted in Fig. 11. Of the 6 stiffness coefficients plotted in Fig. 11, only K_{88} shows significant reduction since it is contributed directly by the stiffness of the pre-tensioned cable member which is cut. The cut made mid-way through the experiment and the resulting transient oscillations towards dynamical equilibrium of the new system is manifested by the varying stiffness coefficients estimated for segments 7–9 (from 7 to 11 s). The identified stiffness coefficients stabilized from segment 10 (11th second) onwards. Based on the identified stiffness coefficients at segments 1 (first) and 15 (last), the change in the stiffness matrix is calculated and used in the *DLV* method to detect damage. Performing *SVD* on the change in stiffness matrix, a set of 4 *DLV*s is identified. Applying these *DLV*s to the reference structural model as nodal displacement vectors, the *NCE* of all elements are computed and the set of *PDE* comprising elements (1, 8) is identified. The current *IDS* therefore comprises elements (1, 8) and *ne*=2.

By omitting readings of the sensor at nodes 9, the readings of the remaining 5 sensors are used to estimate the structural stiffness matrix for different time segments. Comparing the stiffness matrices identified at the first and the last time segments, the change in the stiffness matrix is evaluated. Performing *SVD* on the change in stiffness matrix, a set of 3 *DLV*s is obtained and applied onto the reference model as nodal displacement vectors. The set of *PDE* identified comprises elements (4, 5, 8, 12, 14). Taking the intersection between the set of *PDE* and the current *IDS* which contains elements (1, 8) gives the new *IDS* with element 8 as the only member (*ne*=1). Similarly, by omitting the readings of the sensor at node 1 instead of the sensor at node 9, another set of *PDE* comprising elements (1, 4, 8, 12) is identified. Intersecting the set of *PDE* and the current *IDS* which contains element 8 only gives element 8 as the new *IDS* (*ne*=1). Since the *IDS* for 2 consecutive steps are identical, the iteration is terminated, confirming that the actual damage is in element 8. The whole procedure is summarized in Table 8.

If the raw signals where lost values are padded with zeroes are used instead (that is, without correction), the stiffness matrix at all 15 time segments can still be deduced. However, if *SVD* is performed on the difference in stiffness matrix between the first and the last time segments, no *DLV* is computed. This confirms the necessity of the reconstruction procedure to improve the quality of the measured signals before damage identification procedure can be applied to obtain reliable results.

A comparison between *NCS* and *NCE* is made for this example and the results of their magnitudes are plotted in Fig. 12 for the case of measurements using 6 wireless sensors. The 2 damage indicators, *NCS* and *NCE*, with the corresponding thresholds of 0.1 and 0.01 respectively produce the same conclusion that elements (1, 8) are potentially damaged although the *NCE* measure appears slightly more sensitive by comparing with the values of the square of *NCS*.

5. Observations

In solving for the stiffness matrix in Section 2.3, the premise is that unknowns should not be unnecessarily introduced in large size problems to ensure that reliable results are obtained. Hence it is formulated assuming that the mass matrix is known and is valid if the structure suffers from mild damage and no mass is added to or removed from the structure. In such case, the mass matrix can be evaluated from a finite element model of the reference structure and then substituted into Eq. (11) to form a system of nonlinear equations to solve for the unknown coefficients in the stiffness and damping matrices. If the structure experiences significant change in the mass matrix, then the mass matrix coefficients also need to be estimated. The unknowns in Eq. (11) will increase by $n(n+1)/2$ entries and the number of time steps of acceleration data

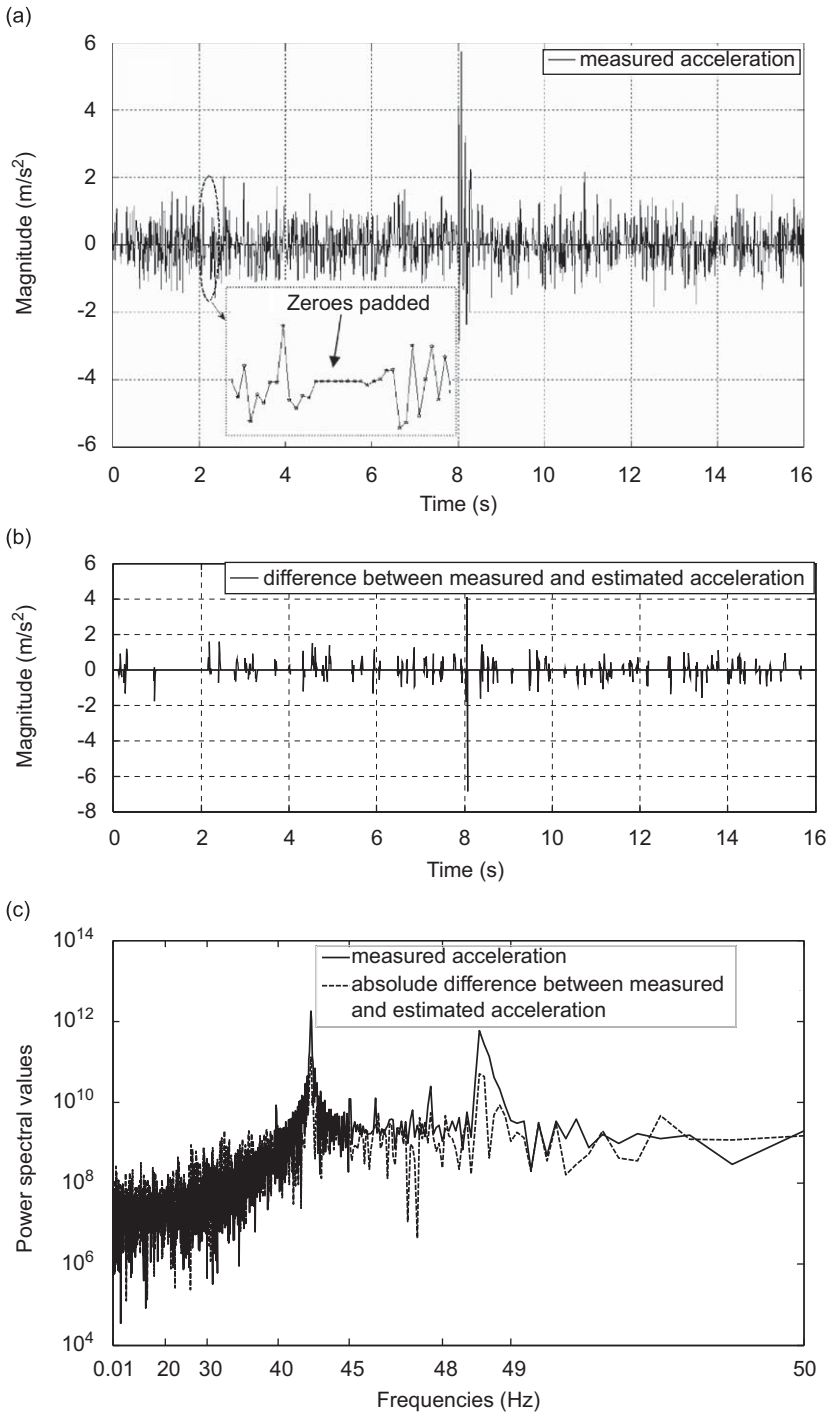

Fig. 10. Comparison between measured and estimated accelerations at sensor node 4 in time (a and b), and frequency (c).

required to solve for the unknown becomes

$$k_1 n \geq \frac{n(n+1)}{2} \times 3 + k_1(n - ns) + 2n + k_1 r \Rightarrow k_1 \geq \frac{n(3n+7)}{2(ns-r)} \tag{12a}$$

To apply the *DLV* method, either displacement or acceleration responses need to be measured. Unless non-contact laser instrument is available, displacement transducers can only be employed if there is a stiff or fixed reference frame on which

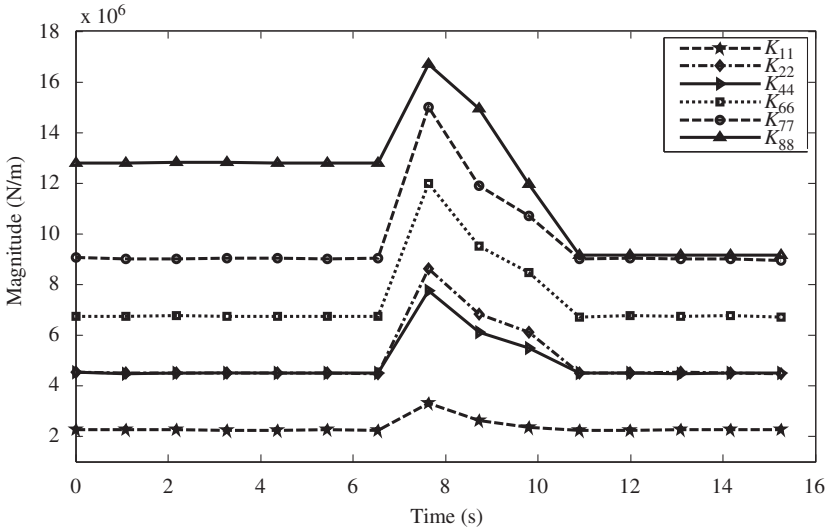

Fig. 11. Variation of structural stiffness coefficients with time.

Table 8
Damage detection of experimental truss structure.

	Set of sensors includes sensors at nodes	No. of *DLV*	*PDE*	Eliminated elements	*IDS*	*ne*
ns=6	[1, 2, 3, 5, 8, 9]	4	[1,8]		[1, 8]	2
k=*ns*−1=5						
i=1	[1, 2, 3, 5, 8]	3	[4, 5, 8, 12, 14]	1	[8]	1
i=2	[2, 3, 5, 8, 9]	3	[1, 4, 8, 12]		[8]	1

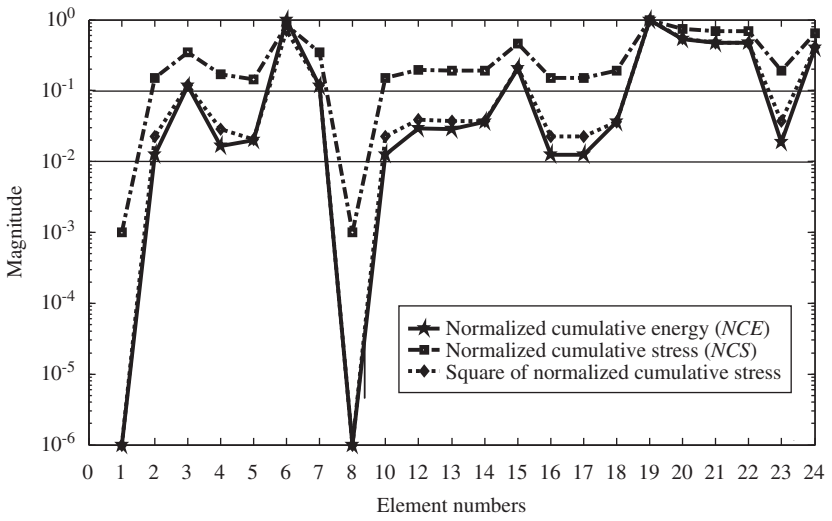

Fig. 12. Comparison between *NCS* and *NCE* for experimental truss (6 wireless sensors are used).

they can be mounted. Since the employment of accelerometers does not require fixed reference frame, they are used in this study to measure acceleration responses. Besides, if the number of measured data points along the time axis (k_1) is fixed, the number of sensors used can be computed following Eq. (12) as

$$ns \geq r + \frac{n(n+3)}{k_1} \tag{12b}$$

Hence, incorporating the requirement of the intersection scheme in Section 2.2, the minimal number of sensors used should be the maximum value between 3 and $[r+n(n+3)/k_1]$. Theoretically, the available sensors should be positioned at critical locations so that maximum information with regards to the safety of the structure can be retrieved. Optimal sensor placement which includes measurement locations and directions has been addressed by other researchers [33–36] and is also relevant to the *DLV* method.

Based on experience with the examples, it is noted that the algorithm can work well for the case of mild degradation in structural parameters with time (less than 0.1 percent reduction within k_1 time steps). The algorithm to compute stiffness matrix from response accelerations is suitable for the online damage detection applications because structural stiffness matrix can be evaluated whenever a set of k_1 measured time steps is available. Perturbations near the time of occurrence of damage (for example, around 7–11 s in the second example) can also be captured, providing additional information.

Using shaker to excite structure dynamically may not be suitable for some types of structures such as bridges, offshore platforms. For cases where shaker is not suitable, other natural modes of excitation such as moving vehicles or ambient sources may need to be considered [37].

6. Conclusions

The *DLV* method which uses the normalized cumulative energy as damage indicator is shown to be applicable for truss and frame structures, the latter comprising members in multi-stress state. To filter out the actual damaged elements from a larger identified potential damaged set, an intersection scheme with the suggested thresholds is proposed and illustrated to be feasible. The importance of using quality signals is demonstrated, where actual signals from wireless sensors, with and without correction, are used with the *DLV* methodology. Numerical and experimental results presented also support the efficiency of the reconstruction algorithm of signals from wireless sensors with up to 25 percent data loss and its suitability to be integrated with the *DLV* method.

References

[1] M.R. Banan, M.R. Banan, K.D. Hjelmstad, Parameters estimation of structures from static response. I. Computational aspects, *Journal of Structural Engineering, ASCE* 120 (1994) 3243–3258.
[2] M.R. Banan, M.R. Banan, K.D. Hjelmstad, Parameters estimation of structures from static response. II. Numerical simulation studies, *Journal of Structural Engineering, ASCE* 120 (1994) 3259–3283.
[3] K.D. Hjelmstad, M.R. Banan, M.R. Banan, Time domain parameters estimation algorithm for structures. I. Computational aspects, *Journal of Structural Engineering, ASCE* 121 (1995) 424–434.
[4] K.D. Hjelmstad, M.R. Banan, M.R. Banan, Time domain parameters estimation algorithm for structures. II. Numerical simulations studies, *Journal of Engineering Mechanics, ASCE* 121 (1995) 435–447.
[5] K.F. Alvin, A.N. Robertson, G.W. Reich, K.C. Park, Structural system identification: from reality to models, *Computers and Structures* 81 (2003) 1149–1176.
[6] J.N. Yang, S. Lin, Identification of parametric variations of structures based on least squares estimation and adaptive tracking technique, *Journal of Engineering Mechanics, ASCE* 131 (2005) 290–298.
[7] D. Bernal, Load vectors for damage localization, *Journal of Engineering Mechanics, ASCE* 128 (2002) 7–14.
[8] F.N. Catbas, D.L. Brown, A.E. Aktan, Use of modal flexibility for damage detection and condition assessment: case studies and demonstrations on large structures, *Journal of Structure Engineering, ASCE* 132 (2006) 1699–1712.
[9] S.T. Quek, P.S. Tua, Q. Wang, Detecting anomaly in beams and plate based on Hibert-Huang transform of real signals, *Smart Materials and Structures* 12 (2003) 447–460.
[10] P.S. Tua, S.T. Quek, Q. Wang, Detection of cracks in plates using piezo-actuated lamb waves, *Smart Materials and Structures* 13 (2004) 643–660.
[11] P.S. Tua, S.T. Quek, Q. Wang, Detection of cracks in cylindrical pipes and plates using piezo-actuated lamb waves, *Smart Materials and Structures* 14 (2005) 1325–1342.
[12] A.K. Pandey, M. Biswas, Damage detection in structures using changes in flexibility, *Journal of Sound and Vibration* 169 (1994) 3–17.
[13] M. Sanayei, S. Scampoli, Structural element stiffness identification from static test data, *Journal of Engineering Mechanics, ASCE* 117 (1991) 1021–1036.
[14] B.H. Oh, B.S. Jung, Structural damage assessment with combined data of static and modal tests, *Journal of Structural Engineering, ASCE* 124 (1998) 956–965.
[15] L. Mevel, A. Benveniste, M. Basseville, M. Goursat, B. Peeters, H.V. Auweraer, A. Vecchio, Input/output versus output-only data processing for structural identification—application to in-flight data analysis, *Journal of Sound and Vibration* 295 (2006) 531–552.
[16] A. Alvandi, C. Cremona, Assessment of vibration-based damage identification techniques, *Journal of Sound and Vibration* 292 (2006) 179–202.
[17] Z.R. Lu, S.S. Law, Features of dynamic response sensitivity and its application in damage detection, *Journal of Sound and Vibration* 303 (2007) 305–329.
[18] D. Bernal, B. Gunes, Flexibility based approach for damage characterization: benchmark application, *Journal of Engineering Mechanics, ASCE* 130 (2004) 61–70.
[19] Y. Gao, B.F. Spencer Jr., D. Bernal, Experimental verification of the flexibility-based damage locating vector method, *Journal of Engineering Mechanics, ASCE* 133 (2007) 1043–1049.
[20] J.P. Lynch, K. Loh, A summary review of wireless sensors and sensor networks for structural health monitoring, *Shock and Vibration Digest* 38 (2006) 91–128.
[21] T. Nagayama, Structural Health Monitoring Using Smart Sensors, Ph.D. Thesis, University of Illinois at Urbana-Champaign, 2007.
[22] K.K. Chintalapudj, Design of Wireless Sensor Network Based Structural Health Monitoring System, Ph.D. Thesis, University of South California, 2006.
[23] Y. Wang, Wireless Sensing and Decentralized Control for Civil Structures: Theory and Implementation, Ph.D. Thesis, Stanford University, 2007.
[24] B.F. Spencer Jr., T. Nagayama, J.A. Rice, Decentralized structural health monitoring using smart sensors, *Proceeding of the SPIE* 6932 (2008) 693202.
[25] S.H. Sim, S.A. Jang, B.F. Spencer Jr., J. Song, Reliability-based evaluation of the performance of the damage locating vector method, *Probabilistic Engineering Mechanics* 23 (2008) 489–495.
[26] J. Juang, R. Pappa, An eigensystem realization algorithm for modal parameter identification and model reduction, *Journal of Guidance, Control, and Dynamics* 8 (1985) 610–627.
[27] R.S. Pappa, K.B. Elliot, A. Schenk, Consistent mode indicator for the eigensystem realization algorithm, *Journal of Guidance, Control, and Dynamics* 16 (1993) 852–858.
[28] J. Juang, *Applied System Identification*, Prentice Hall Inc., Englewood Cliffs, New Jersey, 1994.

[29] D. Bernal, Flexibility-based damage localization from stochastic realization result, *Journal of Guidance, Control, and Dynamics, ASCE* 132 (2006) 651–658.
[30] Y. Gao, B.F. Spencer Jr., Online damage diagnosis for civil infrastructure employing a flexibility-based approach, *Smart Materials and Structures* 15 (2006) 9–19.
[31] P. Wolfe, The secant method for simultaneous nonlinear equations, *Communications of the ACM* 2 (1959) 12–13.
[32] K.J. Bathe, *Finite Element Procedures*, Prentice-Hall Inc., Upper Saddle River, New Jersey, 1996.
[33] K. Worden, A.P. Burrows, Optimal sensor placement for fault detection, *Engineering Structures* 23 (2001) 885–901.
[34] C. Papadimitriou, Optimal sensor placement methodology for parametric identification of structural system, *Journal of Sound and Vibration* 278 (2004) 923–947.
[35] M. Meo, G. Zumpano, On the optimal sensor placement techniques for a bridge structure, *Engineering Structures* 27 (2005) 1488–1497.
[36] M. Liu, W.C. Gao, Y. Sun, M.J. Xu, Optimal sensor placement for spatial lattice structure based on genetic algorithms, *Journal of Sound and Vibration* 317 (2008) 175–189.
[37] J.W. Lee, J.D. Kim, Health monitoring method for bridges under ordinary traffic loadings, *Journal of Sound and Vibration* 275 (2002) 659–667.